Experimental Implementation of Multi-Actuator Vibration Control on an Indoor Walkway

Iván M. Díaz[1], Emma J. Hudson[2], Emiliano Pereira[3], and Paul Reynolds[2,4]

Abstract

Active vibration control (AVC) using inertial mass actuators has been shown to have great potential to mitigate vibrations and to allow the construction of increasingly slender structures leading to significant material savings. Until now, experimental applications have mainly involved the use of SISO (single-input single-output) rather than MIMO (multiple-input multiple-output) strategies. Recently, the authors have proposed a MIMO vibration control methodology based on the velocity-output-feedback concept that considers the dynamics of the inertial actuators and other important issues in human-induced vibrations. This paper details the experimental implementation carried out on an indoor in-service walkway. The experimental programme undertaken involved frequency walking tests, walking tests, heel-drop tests and continuous whole-day in-service monitoring. These measurements enabled the assessment of the vibration control performance, which has been shown to be excellent.

I. Introduction

Improvements in design methods are leading to lighter and slender pedestrian that usually satisfy ultimate limit state criteria but have the potential of attracting complaints coming from excessive human-induced vibrations. Active vibration control (AVC) via inertial mass actuators has been shown to significantly reduce the level of response, allowing structures to satisfy vibration serviceability limits. Up to now, applications mainly involve the use of SISO (single-input single-output) strategies based on collocated control (i.e., the pair sensor/actuator are placed physically at the same point) rather than MIMO (multiple-inputs multiple-outputs) strategies. This is due to the fact that SISO control strategies are easier to design and, unconditional stability and good vibration reduction performance can be achieved under the absence of actuator and sensor dynamics [1]. Although the inclusion of actuator and sensor dynamics makes the stability conditional and degrades the vibration reduction performance, there exist SISO control strategies that mitigate these problems (see for example [2], [3]).

In the case of floor structures, most of the vibration modes are usually locally spatially distributed with closely spaced natural frequencies. This means that there is no single location that can be used to control all the significant modes. Under these circumstances, MIMO control can achieve a better tradeoff between energy consumption and vibration reduction performance, as it was shown in [4], where an optimal placement of actuators and sensors for MIMO control of floor vibrations was presented. The algorithm consists of minimising a performance index (PI) in order to find simultaneously an optimal location of a predefined number of actuator/sensor (A/S) pairs and the feedback gains of direct velocity feedback (DVF) control. The main conclusion of this work is that a MIMO control is more appropriate than SISO and a multi-SISO control. In addition, the algorithm proposed in [4] considers the force/stroke saturation of actuators and a high frequency model of the floor structure, showing that a MIMO control is robust to this saturation and spillover effects.

Recently, the authors have proposed a MIMO vibration control methodology for human-induced vibration based on the velocity-output-feedback concept [5]. This strategy is based on the idea presented in [4] but includes important issues that are important for a successful implementation, such as the dynamics of the inertial actuators, including force and stroke saturation, and the lossy integrators needed to obtain the velocity from the accelerometers. The inclusion of these dynamics is a key point since they significantly affect the stability of the overall system.

This paper details the experimental implementation carried out on an indoor walkway sited at the recently constructed award winning Forum building at the University of Exeter (Exeter, UK). The experimental programme undertaken involved frequency responses tests, walking tests, heel-drop tests and continuous whole-day in-service monitoring. These measurements enabled the assessment of vibration control performance, which has been shown to be excellent. The cumulative distribution function of the response factor has been used to assess the performance of the control system for the whole-day monitoring. Additionally, the vibration dose value (VDV) and the maximum transient vibration value (MTVV) have been computed for comparison.

*The authors acknowledge the financial support provided by the Fundación Caja Madrid through the grant “II Convocatoria de Becas de Movilidad para profesores de las universidades públicas de Madrid durante el curso académico 2012/2013” and also the UK Engineering and Physical Sciences Research Council (EPSRC) though grant EP/J004081/2 entitled “Advanced Technologies for Mitigation of Human-Induced Vibration”

[1]Iván M. Díaz is with ETS Ingenieros de Caminos, Universidad Politécnica de Madrid, ES 28040, Madrid, Spain ivan.munoz@upm.es

[2]Emma J. Hudson and Paul Reynolds are with College of Engineering, Mathematics and Physical Sciences, University of Exeter, EX4 4QF, Exeter, UK E.J.Hudson@exeter.ac.uk,p.reynolds@exeter.ac.uk

[3]Emiliano Pereira and Cristina Alén are with Escuela Politécnica Superior, Universidad de Alcalá, ES 28805, Alcalá de Henares, Madrid, Spain emiliano.pereira@uah.es,cristina.alen@uah.es

[4]Paul Reynolds is with Full Scale Dynamics Limited, 40 Leavygreave Road, S3 7RD, Sheffield, UK p.reynolds@exeter.ac.uk

This work is organised as follows. Section 2 summarises the control scheme used and the design methodology. Section 3 provides the description of the test structure and Section 4 describes the experimental implementation of the design methodology on this structure. The main conclusions of the paper are given in Section 5.

II. Control strategy

A. Control scheme

The general scheme shown in Fig. 1 used to define an optimal DVF MIMO control from the proposed optimisation design process. The dynamics included in Fig. 1 are grouped into the following blocks:

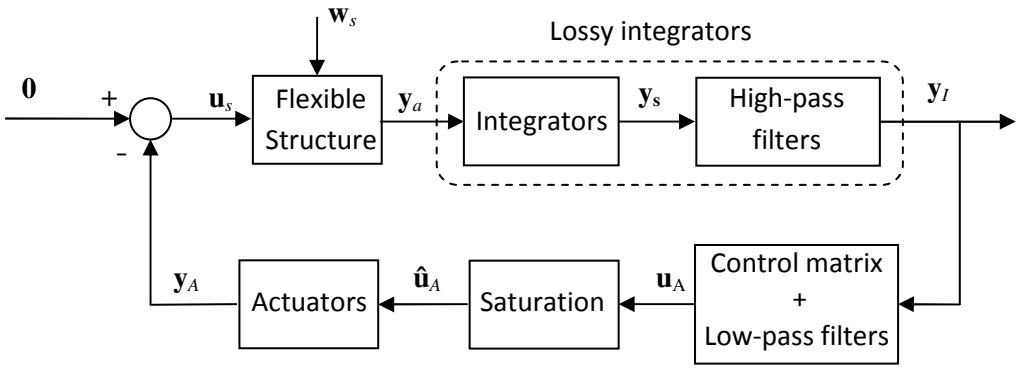

Fig. 1. General control scheme.

1) The structure: modelled by n vibration modes. The inputs are the force generated by p actuators ($\mathbf{u}_s$) and r perturbations ($\mathbf{w}_s$). The accelerations measured by a set of accelerometers at q different locations ($\mathbf{y}_a$) are considered as control outputs.

2) Lossy integrators: needed to obtain the velocity from the accelerometers. The lossy integrators are considered as ideal integrators plus high-pass filters [6]. Thus, each lossy integrator carries out the magnitude and phase shift of an ideal integrator at frequencies above the cut-off frequency of the high-pass filter whilst removing any DC component and avoiding unnecessary high sensitivity to stroke saturation at low frequencies.

For the sake of simplicity, the flexible structure and the integrators are grouped so that the output of the resulting system is $\mathbf{y}_s$, which is the velocity at q locations. Thus, the standard state-space representation of the model for this flexible structure is represented as follows:

$$\begin{aligned} \dot{\mathbf{x}}_s &= \mathbf{A}_s\mathbf{x}_s + \mathbf{B}_{s_1}\mathbf{u}_s + \mathbf{B}_{s_2}\mathbf{w}_s \\ \mathbf{y}_s &= \mathbf{C}_s\mathbf{x}_s. \end{aligned} \tag{1}$$

If model (1) is defined in modal coordinates, the state-space matrices are as follows [7]:

$$\begin{aligned} \mathbf{A}_s &= \begin{bmatrix} \mathbf{0} & \mathbf{I} \\ -\Omega^2 & -2\mathbf{Z}\Omega \end{bmatrix}, \qquad \mathbf{B}_{s_1} = \begin{bmatrix} \mathbf{0} \\ \Phi_u \end{bmatrix}, \\ \mathbf{B}_{s_2} &= \begin{bmatrix} \mathbf{0} \\ \Phi_w \end{bmatrix}, \qquad \mathbf{C}_s = \begin{bmatrix} \Phi_y & \mathbf{0} \end{bmatrix}, \end{aligned} \tag{2}$$

where Ω is a $n \times n$ diagonal matrix formed by the natural frequencies ($[\omega_1, \cdots, \omega_n]$), $\mathbf{Z}$ is a $n \times n$ diagonal matrix formed by the damping ratios ($[\zeta_1, \cdots, \zeta_n]$) and Φ_u, Φ_y and Φ_w are matrices with dimensions $n \times p$, $q \times n$ and $n \times r$, respectively. Each k^{th} column of Φ_u and Φ_w and each row of Φ_y is formed by the k^{th} modal shape values at the positions of the actuators (Φ_u), perturbations (Φ_w) and sensors (Φ_y).

The high-pass filters utilised in this work are second-order Butterworth high-pass filters with cut-off frequency equal to ω_I. The chosen value of ω_I is the result of the tradeoff between the resonance frequency of actuator, since small values of ω_I increase the risk of stroke saturation, and the first vibration mode of the structure, since higher values of ω_I reduce the damping imparted by a DVF controller. The state-space model of each high-pass filter is as follows:

$$\begin{aligned} \dot{\mathbf{x}}_I &= \mathbf{A}_{I_T}\mathbf{x}_I + \mathbf{B}_{I_T}\mathbf{y}_s \\ \mathbf{y}_I &= \mathbf{C}_{I_T}\mathbf{x}_I + \mathbf{D}_{I_T}\mathbf{y}_s, \end{aligned} \tag{3}$$

being the matrices $\mathbf{A}_{I_T} = diag(\mathbf{A}_I, \cdots, \mathbf{A}_I)$, $\mathbf{B}_{I_T} = diag(\mathbf{B}_I, \cdots, \mathbf{B}_I)$, $\mathbf{C}_{I_T} = diag(\mathbf{C}_I, \cdots, \mathbf{C}_I)$ and $\mathbf{D}_{I_T} = diag\left(\omega_I^4, \cdots, \omega_I^4\right)$ block diagonal, where $\mathbf{A}_I$, $\mathbf{B}_I$ and $\mathbf{C}_I$ are defined as follows [8]:

$$\mathbf{A}_I = \begin{bmatrix} 0 & 1 \\ -\omega_I^2 & -2\sqrt{2}\omega_I \end{bmatrix}, \ \mathbf{B}_I = \begin{bmatrix} 0 \\ 1 \end{bmatrix}, \ \mathbf{C}_I = \begin{bmatrix} -\omega_I^4 & -2\sqrt{2}\omega_I^3 \end{bmatrix}. \tag{4}$$

3) The control gain matrix and the required low-pass filters: required to guarantee the finite gain property of the control loop at high frequencies, avoiding spillover problems [9]. The control gain matrix (**K**) in a general form is defined as:

$$K = \begin{bmatrix} K_{11} & K_{12} & \cdots & K_{1q} \\ K_{21} & K_{22} & \cdots & K_{2q} \\ \vdots & \vdots & \ddots & \vdots \\ K_{p1} & K_{p2} & \cdots & K_{pq} \end{bmatrix}, \tag{5}$$

in which K_{pq} is the control gain applied at control input p due to control output q.

The low-pass filters to avoid spillover problems [9] are defined as follows:

$$\begin{aligned} \dot{\mathbf{x}}_{LP} &= \mathbf{A}_{LP_T}\mathbf{x}_{LP} + \mathbf{B}_{LP_T}\mathbf{y}_I \\ \mathbf{y}_{LP} &= \mathbf{C}_{LP_T}\mathbf{x}_{LP}, \end{aligned} \tag{6}$$

being the matrices $\mathbf{A}_{LP_T} = diag(\mathbf{A}_{LP}, \cdots, \mathbf{A}_{LP})$, $\mathbf{B}_{LP_T} = diag(\mathbf{B}_{LP}, \cdots, \mathbf{B}_{LP})$ and $\mathbf{C}_{LP_T} = diag(\mathbf{C}_{LP}, \cdots, \mathbf{C}_{LP})$ block diagonal, where $\mathbf{A}_{LP}$, $\mathbf{B}_{LP}$ and $\mathbf{C}_{LP}$ are defined as follows [8]:

$$\mathbf{A}_{LP} = \begin{bmatrix} 0 & 1 \\ -\omega_{LP}^2 & -2\sqrt{2}\omega_{LP} \end{bmatrix}, \ \mathbf{B}_{LP} = \begin{bmatrix} 0 \\ 1 \end{bmatrix}, \ \mathbf{C}_{LP} = \begin{bmatrix} \omega_{LP}^2 & 0 \end{bmatrix}, \tag{7}$$

The value of ω_{LP}, which is the cut-off frequency, must be sufficiently high when compared with the controlled vibration mode with the maximum resonance frequency.

4) The saturation nonlinearity: models the actuator force limitation, which is limited by the maximum power amplifier input. This maximum value can be decreased to reduce the risk of stroke saturation but also reducing the actuator performance. The outputs of the saturation block, which are the command voltage inputs of the p actuators, are denoted by $\hat{\mathbf{u}}_A$.

5) The inertial-mass actuators: considered are inertial actuators that generate forces through acceleration of an inertial mass to the structure on which it is placed. The linear behaviour of the actuator can be closely described as a third-order dynamic model [10]. Thus, the state space model of the p actuators is as follows:

$$\begin{aligned} \dot{\mathbf{x}}_A &= \mathbf{A}_{A_T}\mathbf{x}_A + \mathbf{B}_{A_T}\hat{\mathbf{u}}_A \\ \mathbf{y}_A &= \mathbf{C}_{A_T}\mathbf{x}_A, \end{aligned} \tag{8}$$

being the matrices $\mathbf{A}_{A_T} = diag(\mathbf{A}_A, \cdots, \mathbf{A}_A)$, $\mathbf{B}_{A_T} = diag(\mathbf{B}_A, \cdots, \mathbf{B}_A)$ and $\mathbf{C}_{A_T} = diag(\mathbf{C}_A, \cdots, \mathbf{C}_A)$ block diagonal, where $\mathbf{A}_A$, $\mathbf{B}_A$ and $\mathbf{C}_A$ are defined as follows [10]:

$$\mathbf{A}_A = \begin{bmatrix} 0 & 0 & \varepsilon\omega_A \\ 1 & 0 & \omega_A^2 + 2\zeta_A\omega_A\varepsilon \\ 0 & 1 & \varepsilon + 2\zeta_A\omega_A \end{bmatrix}, \ \mathbf{B}_A = \begin{bmatrix} 0 \\ 0 \\ g_A \end{bmatrix}, \ \mathbf{C}_A = \begin{bmatrix} 0 & 0 & 1 \end{bmatrix}, \tag{9}$$

where the actuator is defined by $g_A > 0$, its damping ratio ζ_A and natural frequency ω_A. The value of ε models the low-pass properties of the actuator. The actuator in this work is an APS Dynamics Model 400 electrodynamic shaker that has been identified obtaining the following parameters: $\omega_A = 13.2$ rad/s (2.1 Hz), $\zeta_A = 0.5$, $g_A = 12000$ and $\varepsilon = 47.1$.

Thus, the state equation of the closed-loop system is obtained from Fig. 1 and Eqs. (1)-(9), and results in

$$\begin{bmatrix} \dot{\mathbf{x}}_s \\ \dot{\mathbf{x}}_I \\ \dot{\mathbf{x}}_{LP} \\ \dot{\mathbf{x}}_A \end{bmatrix} = \begin{bmatrix} \mathbf{A}_s & \mathbf{0} & \mathbf{0} & -\mathbf{B}_{S_1}\mathbf{C}_{A_T} \\ \mathbf{B}_{I_T}\mathbf{C}_s & \mathbf{A}_{I_T} & \mathbf{0} & \mathbf{0} \\ \mathbf{B}_{LP_T}\mathbf{D}_{I_T}\mathbf{C}_s & \mathbf{B}_{LP_T}\mathbf{C}_{I_T} & \mathbf{A}_{LP_T} & \mathbf{0} \\ \mathbf{0} & \mathbf{0} & \mathbf{B}_{A_T}\mathbf{K}\mathbf{C}_s & \mathbf{A}_{A_T} \end{bmatrix} \begin{bmatrix} \mathbf{x}_s \\ \mathbf{x}_I \\ \mathbf{x}_{LP} \\ \mathbf{x}_A \end{bmatrix} + \begin{bmatrix} \mathbf{B}_s \\ \mathbf{0} \\ \mathbf{0} \\ \mathbf{0} \end{bmatrix} \mathbf{w}_s. \tag{10}$$

The eigenvalues of the $2(n+2q+p) \times 2(n+2q+p)$ state-space matrix are considered into the restrictions defined in the design. These eigenvalues (i.e., the poles of the closed-loop system) are denoted by $\zeta_{CL_\tau}\omega_{CL_\tau} \pm j\omega_{CL_\tau}\sqrt{1-\zeta_{CL_\tau}^2}$, where $\tau \in [1, \cdots, 2(n+2q+p)]$ and j is the imaginary unit.

B. Human vibration perception

The vibration that can be perceived by a human depends on the direction of incidence to the human body, the frequency content of the vibration (for a given amplitude) and the duration of sustained vibration, among other factors. Thus, frequency weighting functions are applied in order to account for the different acceptability of vibrations for different directions and body positions [11]. These have been included in current floor design guidelines such as the SCI guidance [12]. According to ISO 2631 [11], for z-axis vibration and standing and seating, the frequency weighting function (W_k) is a filter with the frequency response shown in Fig. 2. Moreover, sustained vibrations are penalised in the control design, giving more importance to transient vibration of long-duration than those of short-duration. This is taken into account by multiplying the system response by an exponential time weighting (i.e., $e^{\alpha t}$), where $\alpha > 0$ adds a constraint in the relative stability of the controlled system. Note that sustained states are penalised more heavily as α is increased. Therefore, the human vibration perception is considered in the controller design by weighting the state vector of the structure $\mathbf{x}_s = [x_{s_1}, \cdots, x_{s_{2n}}]$ (see (1)) as follows:

$$x_{s_{W_l}} = \left(e^{\alpha t} x_{s_l}(t)\right) * g_{FW}(t),\ l \in [1, \cdots, 2n], \tag{11}$$

where (*) denotes the convolution process and $g_{FW}(t)$ is the impulse response function of a system with the frequency

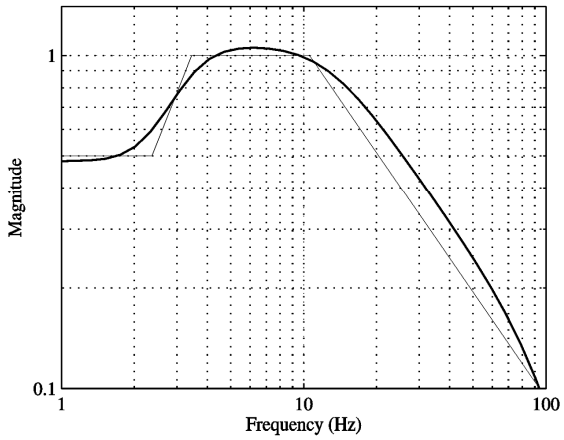

Fig. 2. Frequency weighting function W_k (thicker curve) and its asymptotic definition (thinner curve) [11].

response function (FRF) shown in Fig. 2. Note that the time and frequency weighted vector $\mathbf{x}_{s_W}$ is only used to calculate the PI used to derive the optimal A/S locations and the gain matrix. In other words, the weighting functions are not included in the closed-loop system of Fig. 1.

C. Controller design

The design process is based on the minimisation of a PI related to the dissipation energy of the whole structure due to the AVC action for a given excitation. The PI, which is calculated by using the time and frequency weighted structure states of (11), is defined as follows:

$$J(\mathbf{K}, \Lambda) = \frac{1}{2} \int_0^{t_f} \mathbf{x}_{s_W}^T(\mathbf{K}, \Lambda) \mathbf{Q} \mathbf{x}_{s_W}(\mathbf{K}, \Lambda) dt, \tag{12}$$

where the matrix $\mathbf{Q}$ is a $2n \times 2n$ positive definite matrix and is taken as [4]

$$\mathbf{Q} = \begin{bmatrix} \omega_1^2 \phi_{1,\max}^2 & \cdots & 0 & 0 & \cdots & 0 \\ \vdots & \ddots & \vdots & \vdots & \ddots & \vdots \\ 0 & \cdots & \omega_n^2 \phi_{n,\max}^2 & 0 & \cdots & 0 \\ 0 & \cdots & 0 & \phi_{1,\max}^2 & \cdots & 0 \\ \vdots & \ddots & \vdots & \vdots & \ddots & \vdots \\ 0 & \cdots & 0 & 0 & \cdots & \phi_{n,\max}^2 \end{bmatrix}, \tag{13}$$

in which $\phi_{k,\max}$ is the maximum value of the k^{th} modal shape ϕ_k. Note that the displacement states are weighted by the natural frequencies, thus making the displacement states comparable to the velocity states. The variable Λ contains the locations of a set of p actuators and q sensors. Finally, the value of t_f is the simulation time to obtain the PI, which must be large enough to achieve the steady state of $J(\mathbf{K}, \Lambda)$ (i.e., the weighted vector $\mathbf{x}_{s_W} \cong 0$).

The proposed design methodology is divided into the following steps:

Step 1: Select a set of structure nodes where the p actuators and q sensors can be placed to define each possible combination for actuator and sensors. The set of these possible values for Λ is denoted by Λ_{PI}.

Step 2: Define the following restrictions to minimise the PI $J = (\mathbf{K}, \Lambda)$: i) $\Lambda \in \Lambda_{PI}$, ii) $0 \leq \alpha \leq \min_k (\zeta_k \omega_k)$, $\forall k \in [1, \cdots, n]$, where the upper limit of α ($\min_k (\zeta_k \omega_k)$) guarantees that the system simulation converges to zero, iii) the closed-loop system defined in Eq. (10) is stable (i.e., the possible values for $\mathbf{K}$ are thus defined) and iv) the damping corresponding to the lower closed-loop poles of the actuator dynamics has to be greater than a minimum value denoted as ζ_{stroke}, which is a minimum closed-loop damping to reduce the risk of stroke saturation.

Step 3: Define the system perturbance to assess the controller performance. Note that the design of optimal controllers for unknown disturbances is not trivial since prescribed disturbances are needed within the design process. The solution adopted in this work, similar to that used in [4], is to approximate the influence of zero initial conditions and a spatially distributed, but temporally impulsive, disturbance force by an appropriate initial condition and zero disturbance force. This is achieved by introducing a non-zero initial condition to the velocity states of the structure. Thus, the system perturbance is defined as $\mathbf{x}_s(0) = [x_{s_1} = 0, \cdots, x_{s_n} = 0, x_{s_{n+1}} = \dot{x}_{s_1}(0), \cdots, x_{s_{2n}} = \dot{x}_{s_n}(0)]$, where each value of $\dot{x}_{s_k}(0)$ is obtained as follows:

$$\dot{x}_{s_k}(0) = F_0 \phi_{k,\max}, \tag{14}$$

where F_0 represents the impulse loading applied to a particular vibration mode. Note that the impulsive force is applied to the point of maximum amplitude of each vibration mode, creating thus an extreme scenario for the initial disturbance. It is expected that the control system will perform successfully under other loading conditions.

Step 4: Find the values of Λ and $\mathbf{K}$ that minimise $J(\mathbf{K}, \Lambda)$ of Eq. (12). Operationally, the Step 4 is divided into the following substeps:

Step 4.1: The values of J are obtained for each $\Lambda \in \Lambda_{PI}$ as follows:

$$J_\Lambda = \min_{\mathbf{K}} J(\mathbf{K}, \Lambda), \tag{15}$$

where each J_Λ is calculated by using the MATLAB function *fminsearch*, which minimises the function defined by the simulation of the control scheme of Fig. 1 with the initial conditions defined by Eq. (14), and the restrictions (ii), (iii) and (iv) of Step 2.

Step 4.2: The final values of $\mathbf{K}$ and Λ are those corresponding to the minimum value of J_Λ, which is denoted as J_{OP} and is defined as follows:

$$J_{OP} = \min_{\Lambda} J_\Lambda. \tag{16}$$

III. Structure description

The test structure, which is a walkway sited in the University of Exeter Forum Building (Fig. 3), is approximately 15 m long and 2.7 m wide, as shown in Fig. 4. It was decided that a test grid of 39 test points (TP) would be used (13 x 3 rows) to carry out an experimental modal analysis (EMA) to obtain the structure model (1)-(2). The excitation was provided by an APS Dynamics model 113 shaker, which was placed sequentially at TPs 4 and 7. The acceleration response was monitored by 13 QA-750 accelerometers. Thus, a total of six measurement setups were taken for the modal test: three sets with roving accelerometers for two actuator positions. The FRFs between the structure acceleration and the input force were obtained using a continuous random excitation with frequency band 0-8 Hz. The FRF data obtained were analysed to determine the structural modal properties. Here, the multiple reference polynomial method was used for curve fitting the FRF data.

The properties of the first four modes obtained are presented in Table I and the mode shapes are shown in Fig. 5. The good accuracy of the model can be observed in Fig 6, which shows a comparison between the experimental point accelerance FRF at TP 7 and its regenerated counterpart based on the estimated modal properties. From Table I, it can be observed that the first vibration mode might be excited by the third harmonic of walking excitation (pacing frequency of 2.1 Hz).

TABLE I

Modal properties for the first four vibration modes of the walkway.

Mode Number (bending or torsional)	Natural Frequency (Hz)	Damping Ratio (%)	Modal Mass (Tonnes)	$\phi_{k,\max}$ (m)
1 (bending)	6.3	1.0	15	$66.5 \cdot 10^{-6}$
2 (torsional)	10.5	0.9	10	$98.5 \cdot 10^{-6}$
3 (bending)	14.6	2.1	39	$25.6 \cdot 10^{-6}$
4 (bending)	20.5	2.5	12	$84.8 \cdot 10^{-6}$

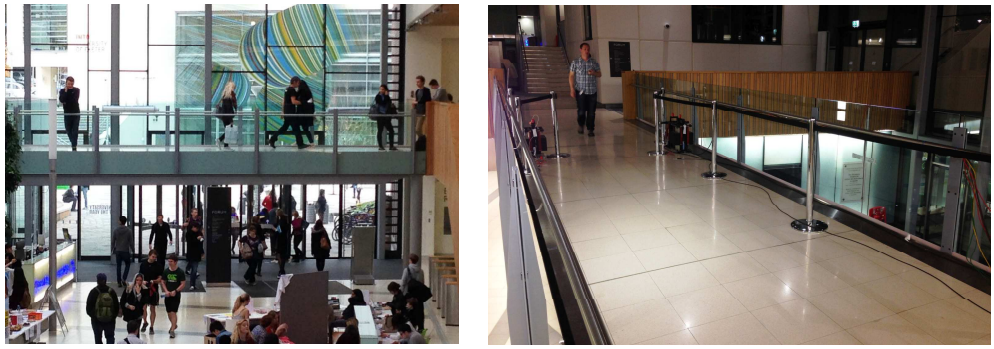

(a) General view. (b) Walking area.

Fig. 3. Forum walkway (University of Exeter).

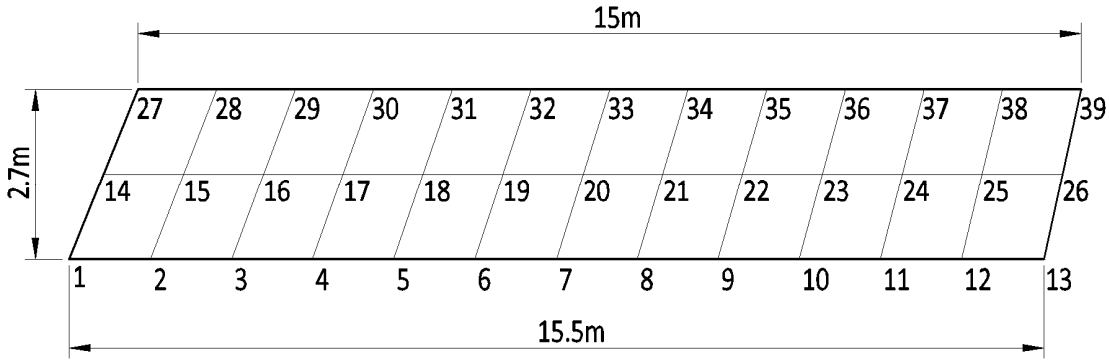

Fig. 4. Test grid for the EMA.

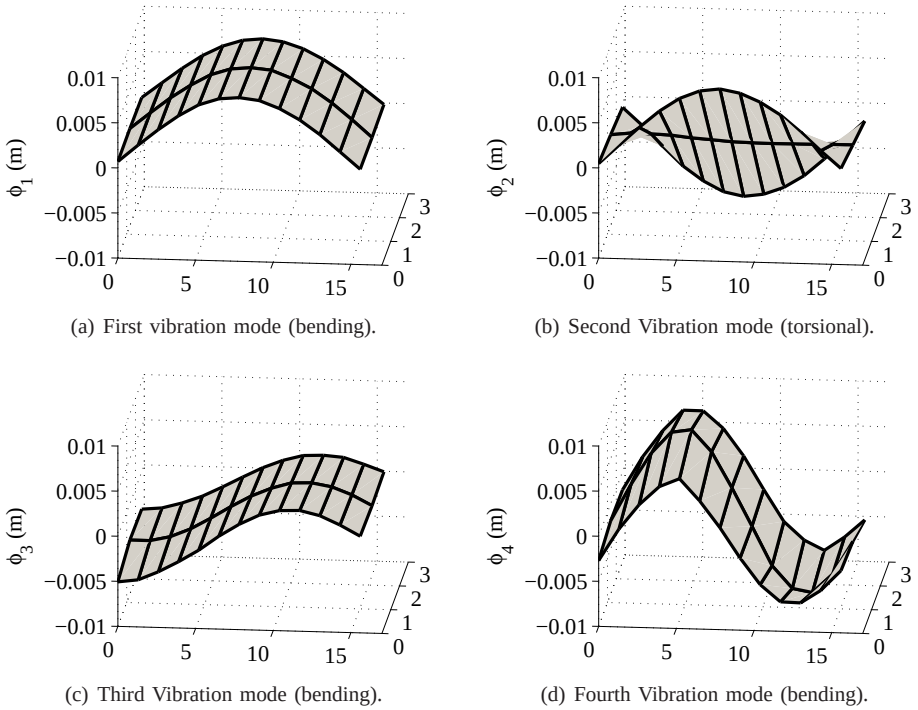

(a) First vibration mode (bending). (b) Second Vibration mode (torsional).

(c) Third Vibration mode (bending). (d) Fourth Vibration mode (bending).

Fig. 5. Mode shapes of the first four vibration modes.

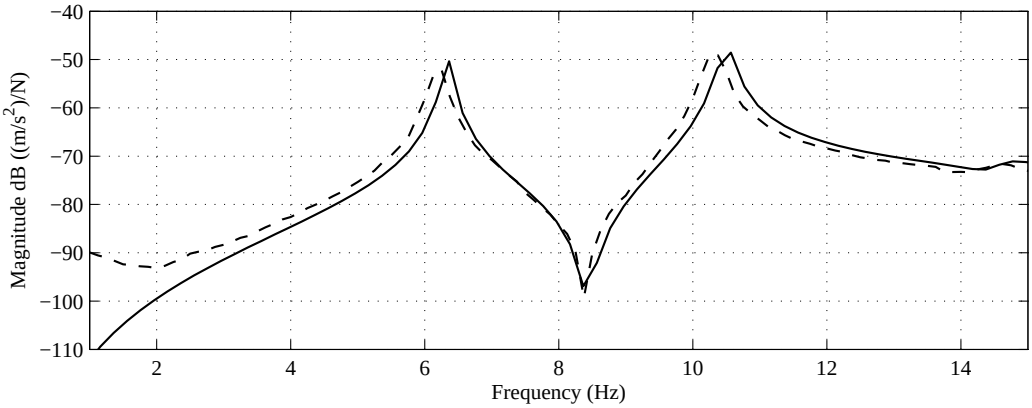

(a) Magnitude in dB referenced to (m/s^2)/N.

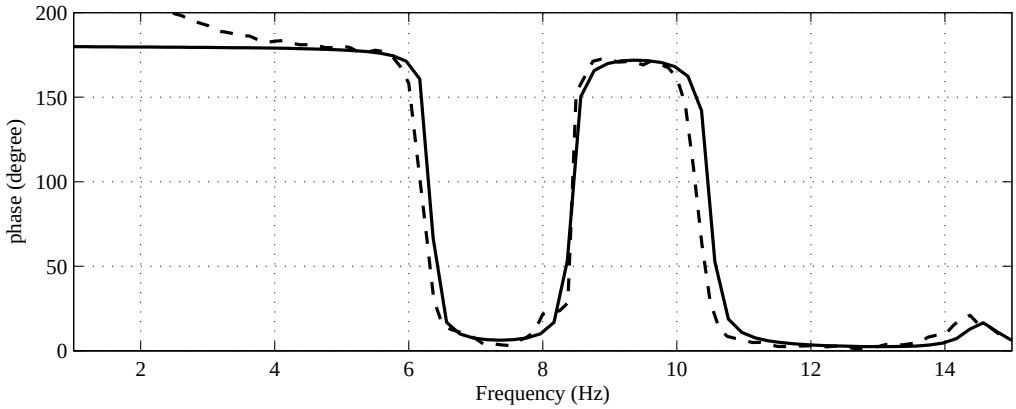

(b) Phase.

Fig. 6. FRF of the Forum walkway at TP 7. (- -) Experimental results and (—) model.

IV. VIBRATION CONTROL PERFORMANCE

The control strategy presented in Section II has been designed to cancel vibrations on the structure described in Section III. Two A/S pairs have been used of this purpose. The designed methodology presented in subsection IIC is now followed. Thus, the following designed parameters have been considered:

- The structural nodes considered in Step 1 are the 39 TPs used to identify the structure dynamics (Fig. 4).
- The restrictions for Steps 2 and 3 used to set the optimisation problem are: $\alpha = 0.25$, $F_0 = 2670$ N (which is the normalised maximum force of an idealised heel-drop excitation).
- The configuration of the control scheme to find the gain matrix **K** consists of setting (see Fig. 1): (i) the actuator saturation voltage which was chosen to be 2 V (this is the maximum allowable value to avoid force saturation of the actuator) and (ii) the cut-off frequency for the high and low-pass filter which were chosen as 2 and 30 Hz, respectively. The high-pass filter at low frequencies reduces the sensitivity of the actuator to stroke saturation and the low-pass filter at high frequencies avoids instabilities due to high-frequency components.

The optimization process describes in Step 4 is then run. The minimum value of the PI is $J_{OP} = 5.695 \cdot 10^{-2}$ for the A/S pairs placed at TPs 7 and 8 with $K_{11} = 755$ and K_{22}= 741. For this particular structure, K_{12} was -2, which influence on the control scheme is very small, and then it can be neglected in the practical implementation.

A. Frequency response tests

The AVC system was assessed firstly by carrying out FRF-based tests. The actuators were placed at TPs 7 and 8, an excitation shaker was placed at TP 7 and several accelerometers were distributed along the structure. Fig. 7 shows the experimental FRFs with and without control between TP 4, 7 and 10 and TP 7. The maximum reduction achieved was almost 30 dB for the first vibration mode and 17 dB for the second one. Apart from the less sensitive to excitation, the maximum values of the FRF magnitude has decreased in such a way that is much more difficult to excite the structure by pedestrian excitations. It is important to observe that the controlled structure is not sensitive to excitation close to the natural frequency of the actuator. That is, the controlled system is insensitive to stroke saturation.

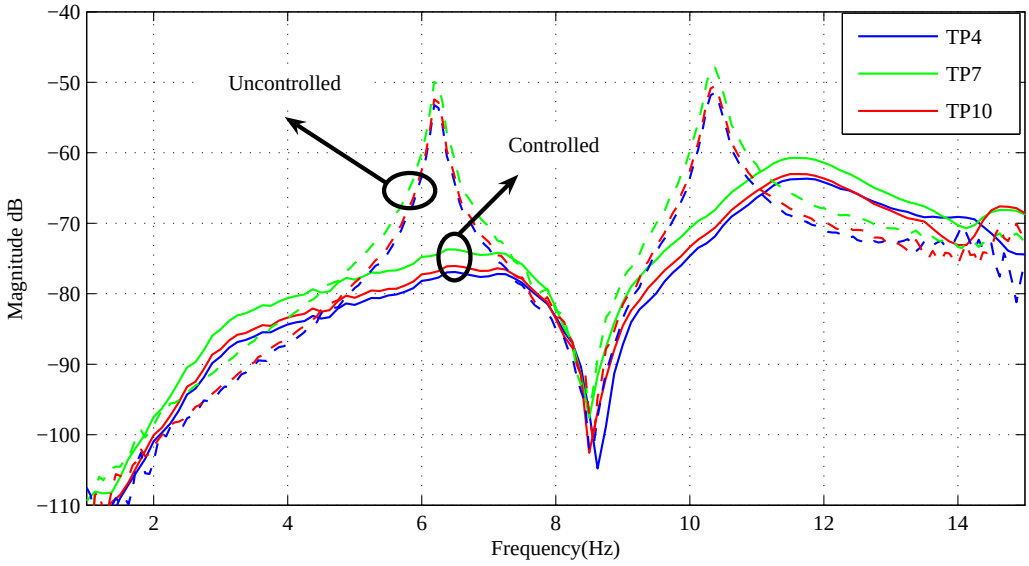

Fig. 7. FRF-acceleration/force.

B. Time history tests

The structure vibration level was measured by carrying out single pedestrian tests of walking at 2.1 Hz in such a way that the first vibration mode of the structure was excited by the third harmonic of walking. The tests consist of walking from one side to the other and back again. The pacing frequency was controlled using a metronome set to 126 beats per minute. Fig. 8 shows an example of W_k weighted response acceleration time histories (including the 1-s running RMS acceleration) for an uncontrolled and controlled test. The maximum transient vibration value (MTVV) calculated from the maximum value of running RMS acceleration is used to compared results. MTVV value was reduced by approximately 85 % for the controlled test. The response factor (R-factor is usually used) to assess the vibration serviceability of structures. This

R-factor is obtained by dividing the MTVV by 0.005 m/s^2. Then R-factor for the uncontrolled test was 20.4 and 3.2 for the controlled test.

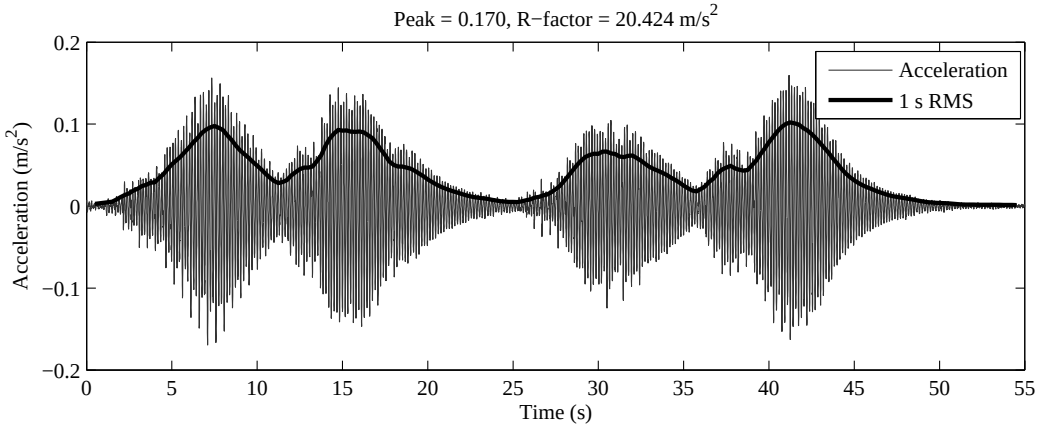

(a) Uncontrolled.

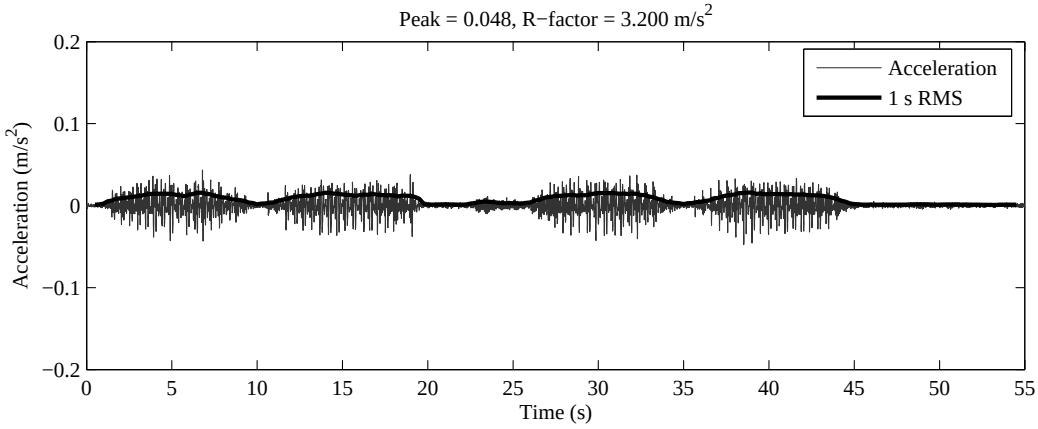

(b) Controlled.

Fig. 8. Experimental results. Walking at 2.1 Hz (126 bpm).

The performance was also tested by using heel-drop excitations, which is an impulsive excitation useful in evaluation of floor structures. A heel-drop excitation is the force created by a person standing on their toes and suddenly dropping to their heels to hit the floor. Fig. 9 shows an example of performance. It can be observed that 17 signal cycles are needed to reduce the acceleration level under 0.05 m/s^2; however, only 2 signal cycles are needed for the controlled case.

C. Whole day monitoring

Continuous whole-day monitoring tests were also carried out to assess the vibration reduction under real in-service loading. The acceleration was measured from 10:00 am to 17:00 pm during two working days, one day without and one with the AVC system working (see Fig. 10). The R-factor and the VDV are used to quantify the vibration reduction. The cumulative distribution of the R-factor is shown in Fig. 11 for TPs 4, 7 and 10 for the controlled and uncontrolled case. The proportion of time that the acceleration was over an R-factor of 4 was 20 % without control, whereas the inclusion of the control decreases this value to an impressive 0.2 %.

For walking activities are, by their nature, not continuous, i.e., they are intermittent. Thus, for intermittent vibrations, the cumulative VDV is generally accepted to be a reliable quantity in determining perceptive tolerance levels [12]. Fig. 12 shows the cumulative distribution of the VDV for the same TPs and with and without control. Considering 7 hours of continuous monitoring, the VDV is reduced from 0.467 to 0.159 m/s$^{1.75}$ and for 16 hours, the VDV is reduced from 1.270 to only 0.432 m/s$^{1.75}$.

V. Conclusions

This work has presented the experimental implementation of a MIMO AVC on an in-service structure. The AVC methodology has been recently proposed by the authors and has considered the most important issues that have to be taken into account in a successful implementation. This point has been demonstrated by undertaking an experimental programme

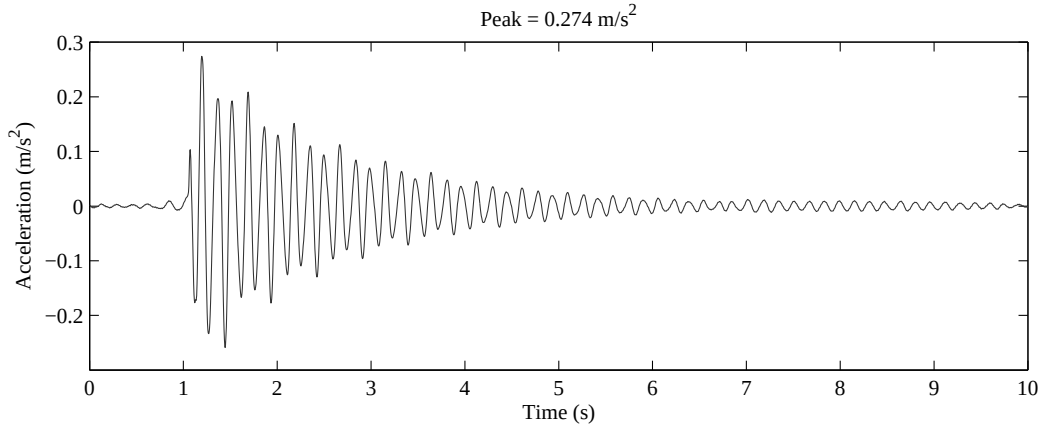

(a) Uncontrolled.

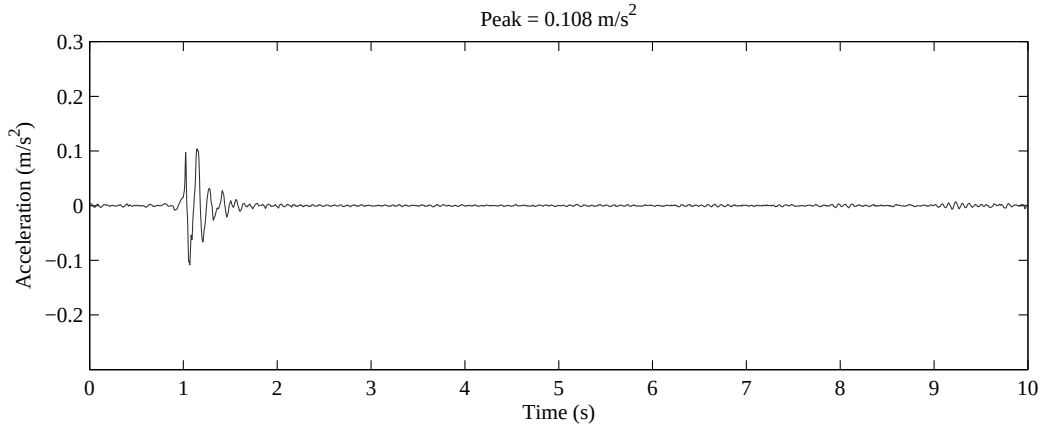

(b) Controlled.

Fig. 9. Experimental results. Heel drop.

involving frequency responses tests, walking tests, heel-drop tests and continuous whole-day in-service monitoring. All the tests carried out have demonstrated the AVC capacity of reducing vibration. As an example, the cumulative R-factor for a whole-day monitoring was computed. The portion of time that an R-factor of 4 was exceeded was approximately 20 %. This value was reduced to an impressive 0.2 % when the AVC system was working.

ACKNOWLEDGMENT

The authors acknowledge the financial support provided by the Fundación Caja Madrid through the grant “II Convocatoria de Becas de Movilidad para profesores de las universidades públicas de Madrid durante el curso académico 2012/2013” and also the UK Engineering and Physical Sciences Research Council (EPSRC) though grant EP/J004081/2 entitled “Advanced Technologies for Mitigation of Human-Induced Vibration”. The authors would also like to thank Mr Wai Kei Ao, Mr Vasileios Karakonstantis, Miss Jie Niu and Dr Donald Nyawako for their help in the experimental work.

Dr. Iván M Díaz would like to acknowledge Erasmus for Training Programme for covering partly his costs during his short stay at the University of Exeter.

REFERENCES

[1] M. J. Hudson and P. Reynolds, “Implementation considerations for active vibration control in the design of floor structures,” *Engineering Structures*, vol. 44, pp. 334–358, 2012.

[2] I. M. Díaz, E. Pereira, and P. Reynolds, “Integral resonant control scheme for cancelling human-induced vibrations in light-weight pedestrian structures,” *Structural Control and Health Monitoring*, vol. 19, pp. 55–69, 2012.

[3] I. M. Díaz, E. Pereira, M. J. Hudson, and P. Reynolds, “Enhancing active vibration control of pedestrian structures using inertial actuators with local feedback control,” *Engineering Structures*, vol. 41, no. 1, pp. 157–166, 2012.

[4] L. M. Hanagan, E. C. Kulasekere, K. S. Walgama, and K. Premaratne, “Optimal placement of actuators and sensors for floor vibration control,” *Journal of Structural Engineering*, vol. 126, no. 12, pp. 1380–1387, 2000.

[5] E. Pereira, I. M. Díaz, E. J. Hudson, and P. Reynolds, “Optimal control-based methodology for active vibration control of pedestrian structures,” *Engineering Structures (submitted for publication)*.

[6] S. S. Aphale, A. J. Fleming, and S. O. R. Moheimani, “Integral resonant control of collocated smart structures,” *Smart Materials and Structures*, vol. 16, no. 2, pp. 439–446, 2007.

[7] W. K. Gawronski, *Advanced Structural Dynamics and Active Control of Structures*. Springer-Verlag, 2004.

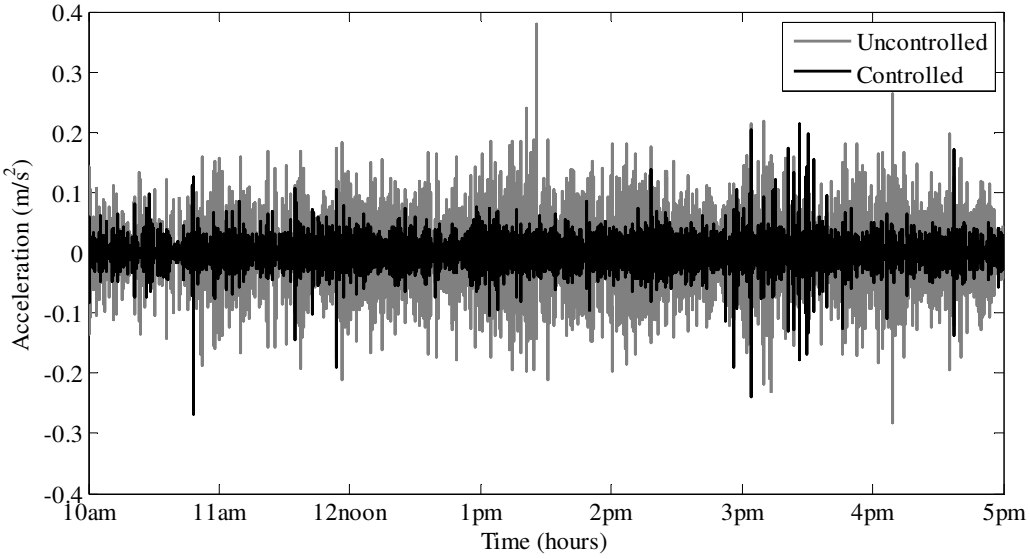

Fig. 10. Experimental results. Group random walking.

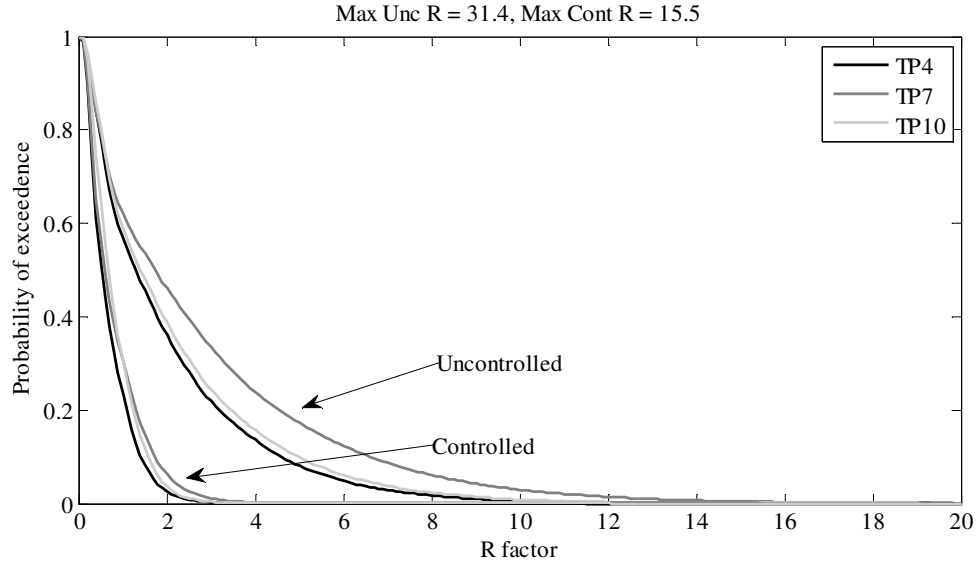

Fig. 11. Experimental results. R-factor monitoring.

[8] J. Middlehurst, *Practical Filter Design*. Prentice Hall, 1993.
[9] W. M. Griggs, D. O. B. Andersona, and A. Lanzon, "Amixed small gain and passivity theorem in the frequency domain," *Systems and Control Letters*, vol. 56, no. 9-10, pp. 596–602, 2007.
[10] I. M. Díaz and P. Reynolds, "Acceleration feedback control of human-induced floor vibrations," *Engineering Structures*, vol. 32, no. 1, pp. 163–173, 2010.
[11] ISO2631-1, *Mechanical vibration and shock - Evaluation of human exposure to whole-body vibration. Part 1: General requirements*. International Organization for Standardization, 1997.
[12] A. L. Smith, S. J. Hicks, and P. J. Devine, *Design of floors for vibration: A new approach (P354)*. The Steel Construction Institute, 2007.

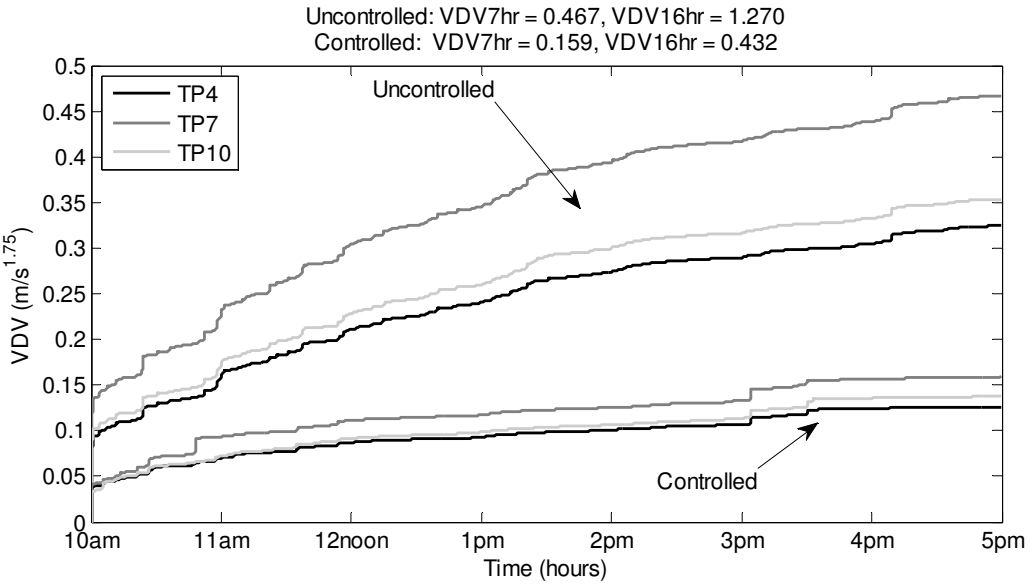

Fig. 12. Experimental results. VDV monitoring.